Clinical Radiology 74 (2019) 813.e19–813.e27

Contents lists available at ScienceDirect

Clinical Radiology

journal homepage: www.clinicalradiologyonline.net

Texture analysis of multi-phase MRI images to detect expression of Ki67 in hepatocellular carcinoma

Y. Li [a,*,1], C. Yan [a,1], S. Weng [b], Z. Shi [a], H. Sun [a], J. Chen [a], X. Xu [a], R. Ye [a], J. Hong [c]

[a] *Department of Radiology, First Affiliated Hospital of Fujian Medical University, Fuzhou, Fujian, 350005, China*
[b] *Department of Radiology, Fujian Provincial Maternity and Child Health Hospital, Fuzhou, Fujian, China*
[c] *Department of Radiation Oncology, First Affiliated Hospital of Fujian Medical University, Fuzhou, Fujian 350005, China*

ARTICLE INFORMATION

Article history:
Received 10 January 2019
Accepted 24 June 2019

AIM: To determine whether texture analysis of preoperative magnetic resonance imaging (MRI) images could be used to detect Ki67 expression, a widely used cell proliferation marker in hepatocellular carcinoma (HCC).

MATERIALS AND METHODS: In total, 83 patients were included, 25 with low Ki67 (Ki67 $\leq$10%) HCC expression and 58 with high Ki67 (Ki67 $\geq$10%) HCC expression as demonstrated by retrospective surgical evaluation. All patients were examined using a 3 T MRI unit with one standard protocol. The region of interest was drawn manually by one radiologist. Texture analysis included histogram, co-occurrence matrix, run-length matrix, gradient, auto-regressive model, and wavelet transform features as calculated by MaZda (version 4.6; quantitative texture analysis software). The features reduced by the Fisher, probability of classification error, and average correlation coefficient (POE+ACC), mutual information were used to select the features that predicted Ki67 proliferation status with highest accuracy and then using the B11 program for data analysis and classification.

RESULTS: The misclassification rate of the principal component analysis (PCA) in the hepatobiliary phase (HBP), T2-weighted imaging (T2WI), arterial phase (AP), and portal vein phase (PVP) was 36/83 (43.37%), 35/82 (42.68%), 40/83 (48.19%), and 34/83 (40.96%), respectively. The misclassification of the linear discriminant analysis in HBP, T2WI, AP, and PVP phase was 13/83 (15.66%), 21/82 (25.61%), 9/83 (10.84%), and 8/83 (9.64%), respectively. The misclassification of the nonlinear discriminant analysis in HBP, T2WI, AP, and PVP phase was 7/83 (8.43%), 6/82 (7.32%), 5/83 (6.02%), and 7/83 (8.43%), respectively.

CONCLUSIONS: Texture analysis of HBP, AP, and PVP were helpful for predicting Ki67 expression and may provide a less-invasive method to investigate critical histopathology markers for HCC.

* Guarantor and correspondent: Y. Li, Department of Radiology, The First Affiliated Hospital of Fujian Medical University, Fuzhou, 350005, Fujian, China. Tel.: +86 18959172818; fax: +86 59183318716.
E-mail address: fjmulym@163.com (Y. Li).
[1] Chuan Yan and Yueming Li contributed equally to this work and are joint first authors.

https://doi.org/10.1016/j.crad.2019.06.024
0009-9260/

Introduction

Hepatocellular carcinoma (HCC) is a global health problem, which is ranked as the sixth most common neoplasm and the third leading cause of cancer-related death.[1] Despite the improving prognosis of patients with HCC due to advances in diagnosis and treatment, the overall survival is still low due to the high rate of recurrence after curative treatment.[2,3] HCC recurrence at 5 years affects 70% of cases, reflecting either intrahepatic metastases or multicentric recurrence, in 25% of cases after liver transplantation.[4] Several studies have shown that the prognostic factors of HCC include cirrhosis, chronic active hepatitis, and hepatitis C virus (HCV) positivity.[5] Additionally, tumour factors, such as tumour size, histological differentiation, macro- or micro-vascular invasion, and microsatellite nodules,[6,7] and treatment strategies, such as liver transplantation, hepatic resection, and radiofrequency ablation,[8,9] have also demonstrated efficacy as prognostic indicators.

Uncontrolled cell proliferation is the most important characteristics of cancer.[10] Ki67 is a nuclear antigen that is associated with cell proliferation activity. It is one of the most widely used proliferation-associated markers in cancer cells.[11] The proliferation status of a neoplasm is related to the biological behavior of the tumour and may indicate the effect of treatment and prognosis. The elevated expression of Ki67 is closely associated with tumour aggressiveness and higher mortality.[12] Recently, a study reported that high Ki-67 was associated with poor disease-free survival, relapse-free survival, and overall survival.[13] Thus, it is suggested that Ki67 may be a valuable biomarker for clinical deterioration and the prognosis of an HCC patient.[13,14]

Currently, pathological methods are commonly used to obtain information about tumour proliferation status by surgical tissue resection; however, operative treatment is limited by tumour size, location, liver function, and performance status in patients with HCC.[15] In clinical practice, the diagnosis of HCC is usually determined by the alpha-fetoprotein level (AFP), contrast-enhanced computed tomography (CECT), or magnetic resonance imaging (MRI).[16] Although conventional imaging techniques, such as the aforementioned CECT/MRI, cannot detect Ki67 expression directly, there remains a need for the non-invasive prediction of Ki67 proliferation from preoperative methods.

Texture analysis is a sophisticated imaging technique that can generate extensive data from medical imaging.[17] These texture features can represent the lightness, uniformity, density, roughness, regularity, coarseness, randomness, fineness, smoothness, granulation, etc.,[18] which may reflect the underlying structure and characteristics of tumours normally only detectable at histopathology.[19] Texture analysis has been successfully applied in several studies including liver fibrosis,[20] breast cancer,[21] renal neoplasm,[22] and others.

To the authors' knowledge, texture analysis has not been investigated as a tool for discriminating the expression of Ki67 in HCC. Thus, the aim of the present study was to retrospectively evaluate the accuracy of texture analysis derived from MRI to discriminate Ki67 proliferation status in HCC.

Material and methods

Patients

This retrospective study was approved by the institutional review board of the hospital, who deemed that the requirement for informed consent could be waived. Participants were enrolled in the study between September 2014 and November 2017 according to the following inclusion criteria: (1) histopathologically confirmed HCC at surgery; (2) liver MRI examination including hepatobiliary phase (HBP) and contrast-enhanced imaging performed at First Affiliated Hospital of Fujian Medical University, Fuzhou, Fujian, China; and (3) the immunohistochemical detection of Ki67 was available from the histopathology report. Exclusion criteria included (1) poor MRI image quality due to severe artefacts in the hepatobiliary phase images and/or contrast-enhanced images (n=5), 2) local treatment before MRI examination (n=7), and (3) MRI performed using a different 3 T MRI machine (n=13). Finally, 83 patients (72 men, 11 women; median age, 52 years; range, 23–85 years) were included in this retrospective study. The flow diagram for the inclusion and exclusion criteria of the study is shown in Fig 1. Twenty-five patients were categorised as the "low Ki67 HCC group" (Ki67 $\leq$10%), whereas the remaining 58 patients were categorised as the "high Ki67 HCC group" (Ki67 $>$10%). After classification the electronic medical record (EMR) was searched and the relevant clinical information of the participating patients was retrieved for presentation in this study (Table 1).

MRI examination

All MRI examinations were performed using a 3 T MRI machine (MAGNETOM Verio; Siemens, Healthcare, Erlangen, Germany) with a dedicated phased-array body coil. The standard abdominal MRI protocol consisted of the following sequences: (1) axial T2-weighted fat-suppressed turbo-spin-echo (TSE): 4,700 ms repetition time (TR)/79 ms echo time (TE), 5 mm section thickness, 1 mm intersection gap, 21×38 field of view (FOV); (2) in-phase and out-of-phase axial T1-weighted imaging: 133 ms TR/2.5 ms (in-phase), 6.2 ms (out-phase) TE, 5 mm section thickness, 1 mm intersection gap, 21×38 FOV; (3) diffusion-weighted imaging (DWI, b=50, 800 s/mm^2) performed with a free-breathing single-shot echo-planar technique, 9,965 ms TR, 73 ms TE, 5 mm section thickness, 1 mm intersection gap, 21×38 FOV. Corresponding ADC maps were automatically calculated by the MRI system; and (4) dynamic contrast enhanced MRI, a three-dimensional (3D) gradient echo sequence with volumetric interpolated breath-hold examination (VIBE), was performed before and after injection of gadobenate dimeglumine (MultiHance; Bracco, Shanghai,

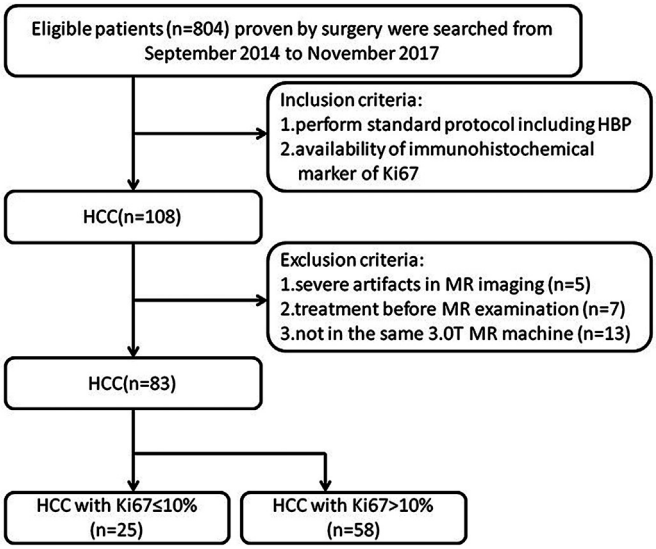

Figure 1 Flowchart of the study selection process.

China) 0.2 ml/kg at a rate of 2 ml/s followed by a 20 ml saline flush with the following parameters: 3.9 ms TR, 1.4 ms TE, 3 mm section thickness, no intersection gap, 25×38 FOV. Hepatic arterial phase (AP), portal venous phase (PVP), equilibrium phase images, and hepatobiliary phase (HBP) were obtained at 20–30, 70–80, 180 seconds and 90 minutes after contrast medium injection, respectively.

Table 1
Baseline characteristics of the study population.

Parameter	Low Ki67 group (n=25)	High Ki67 group (n=58)	p-Value
Age (years)[a]	53.56±12.97	53.40±11.59	0.95
Sex			0.9
Male	21 (25.3)	51 (61.5)	
Female	4 (4.8)	7 (8.4)	
Aetiology of liver disease			0.895
Hepatitis B virus	21 (25.3)	51 (61.5)	
None or other	4 (4.8)	7 (8.4)	
Liver cirrosis			0.268
Present	16 (19.3)	44 (53.0)	
Absent	9 (10.8)	14 (16.9)	
No. of tumours			0.764
One	20 (24.1)	48 (57.8)	
Two	5 (6.0)	10 (12.1)	
AFP >20 ng/ml			0.032
Present	13 (15.6)	44 (53.0)	
Absent	12 (14.5)	14 (16.9)	
ALT (U/L)[a]	48.96±46.10	72.26±190.25	0.548
AST (U/L)[a]	40.04±25.05	58.93±98.12	0.347
ALT/AST[a]	1.21±0.48	1.11±0.62	0.486
Edmondson–Steiner grade			<0.001
I	3 (3.6)	0 (0)	
II	21 (25.3)	30 (36.2)	
III	1 (1.2)	28 (33.7)	

Unless otherwise indicated, data are numbers of patients, with percentage in parentheses.
ALT, alanine aminotransferase level; AST, aspartate aminotransferase level; AFP, alphafetoprotein.
[a] Data are means±standard deviation.

Imaging feature evaluation

All MRI images were reviewed in the picture archiving and communication system (PACS). Two radiologists assessed the imaging features of the HCC or largest lesion (in the case of multiple lesions) by consensus. The imaging features were selected according to the Liver Imaging-Reporting and Data System (LI-RADS 2017) diagnostic algorithm (https://www.acr.org/Clinical-Resources/Reporting-and-Data-Systems/LI-RADS) including major features (arterial enhancement, washout appearance, capsule appearance) and ancillary features (mild-moderate T2 hyperintensity, restricted diffusion, intralesional fat, blood products, etc.).[23] Maximum tumour diameter on the axial HBP images or other phases where lesions was shown more clearly were additionally used in case of artefact.

Texture analysis and feature selection

MaZda software (version 4.6, available at http://www.eletel.p.lodz.pl/mazda/) was used for texture analysis.[24,25] All images were transformed into digital imaging and communications in medicine (DICOM) format for compatibility with MaZda. One radiologist manually drew the irregular region of interest (ROI) on the section containing the largest proportion of tumour that was most representative. HBP or T2-weighted imaging (in case of artefact) were first for analysis. Subsequently, the ROI was copied onto other phase images as required. If the tumour location had changed due to respiratory movement, fine adjustments were made to the ROI. Grey-level normalisation was conducted in each ROI to minimise the influence of contrast variation and brightness using the method that normalises image intensities in the range $\mu \pm 3SD$ (μ grey level mean, SD standard deviation). The extracted texture features included the following: grey-level histogram (information about the intensity of pixels on the image without any spatial relations), the grey-level co-occurrence matrix (GLCOM, information about the grey-level value distribution of pairs of pixels, separated by a defined distance in a given direction), the grey-level run-length matrix (GLRLM, information about pixel runs with the same grey level values in a given direction and depicts intensity homogeneity in given direction), the absolute gradient (GRA, information about the spatial variation of grey level values), the autoregressive model (ARM, depiction of texture based on the statistical correlation between neighboring pixels), and wavelet transform (information about the frequency of similar intensity and depicts the wavelet transform of the pixels).[25,26] More detailed texture features are listed in Table 2. All of these features were derived from HBP, AP, PVP, and T2-weighted images (T2WI). Feature selection algorithms included (Fisher coefficient, mutual information [MI], and classification error probability combined with average correlation coefficients [POE + ACC]). These were combined for the identification of 30 texture features in total, with the highest discriminative power for classification. The correlation between the 30 texture features

Table 2
List of texture features.

Main features	More detailed features
Grey-level histogram	Mean, variance, skewness, kurtosis, percentiles (1, 10, 50, 90, 99%)
Grey-level co-occurrence matrix (GLCOM)	Angular second moment, contrast, correlation, entropy, sum entropy, sum of squares, sum average, sum variance, inverse difference moment, difference entropy, difference variance (for four directions and five interpixel distances (offsets; n=1–5))
Grey-level run-length matrix (GLRLM)	Run-length non-uniformity, grey-level non-uniformity, long run emphasis, short run emphasis, fraction of image in runs (for four angles)
Absolute gradient (GRA)	Gradient mean, variance, skewness, kurtosis, non-zeros
Autoregressive model (ARM)	Teta 1–4, sigma
Wavelet transform	Energies of wavelet transform coefficients in sub-bands LL, LH, HL, HH

derived from HBP, AP, PVP, T2WI, and Ki67 were also calculated.

Histopathological analysis

Histopathological evaluation was available after hepatectomy for HCC across all patients. At the participating hospital, all surgical specimens were routinely fixed in 10% formaldehyde solution, and 2 μm thick sections were acquired every 5 mm. Two pathologists who were blind to MRI information jointly evaluated the surgical specimens. A commercially available monoclonal mouse anti-human Ki67 antibody was used for immunohistochemical labeling of Ki67. The Ki67 labeling index (LI) was calculated according to the percentage of immunoreactive cells observed under 10 high-power fields (×400) in every case. The average value was carried out in the areas with positive nuclei (hot spot) within the tumour. According to the results, HCC cases were classified into "low Ki67 group (Ki67 ≤10%)" and "high Ki67 group (Ki67 >10%)" categories.[27]

Statistical analysis and tissue classification

Statistical analyses were performed using SPSS (version 19.0, SPSS, Chicago, IL, USA). Baseline characteristics of the patients were recorded as mean and standard deviation or count and proportion. Continuous variables were compared with Student's t-test or the Mann–Whitney U-test if not normally distributed. Categorical variables were compared using Pearson's chi-squared test or Fisher's exact test. The correlations between texture parameters derived from HBP, AP, PVP, and T2WI, and Ki67 LI were evaluated using Spearman's rank-correlation test, respectively. In all instances, a p-value of <0.05 was considered statistically significant.

The B11 module of the MaZda (version 4.6) software package was used for texture data analysis and classification. Principal component analysis (PCA), linear discriminant analysis (LDA), and nonlinear discriminant analysis (NDA) were used to reduce the feature vector dimension and increase the discriminative power. Raw data analysis (RDA), PCA, LDA, and NDA were run based on the best 30 texture features. The classifier 1–nearest neighbour (1-NN) was used for the most expressive features resulting from PCA analysis, the most discriminating features resulting from LDA analysis, and the artificial neural network classifier for features resulting from NDA analysis. The misclassification rate is defined as total false samples divided by the total samples and the false sample means that the estimated Ki67 group is different from the observed Ki67 group. The classification results were arbitrarily divided into several levels according to the misclassification rates: excellent (misclassification rates ≤10%), good (10% <misclassification rates ≤20%), moderate (20% <misclassification rates ≤30%), fair (30% <misclassification rates ≤40%), and poor (misclassification rates >40%).[22]

Results

The baseline characteristics of the 83 patients are summarised in Table 1. There were significant differences for AFP value between the low and high Ki67 groups (p=0.032). The Edmondson–Steiner tissue grade (grades I–III) were also statistical difference between the two groups ($p<0.001$).

MRI feature evaluation

The morphological characteristics between the low and high Ki67 groups are described in Table 3. Tumour size and haemorrhage rates were statistically different (p=0.026, p=0.003, respectively) between the two groups. Moreover, there was a significant correlation between tumour size and Ki67 LI (rho=0.246, p=0.025); however, no statistically significant differences were detected between the two groups for imaging features such as arterial phase hyperenhancement, hepatobiliary phase hypo-intensity, etc.

Texture analysis and tissue classification

The texture parameters including histogram, GLCOM, GLRLM, GRA, ARM, and wavelet transform were generated as presented in Figs 2 and 3. The correlation between 30 different texture features derived from HBP, AP, PVP, T2WI, and Ki67 LI were listed in Table 4 alongside statistical results. Some of the 30 texture features were omitted from the table for brevity. The data demonstrated a clear and significant correlation between arterial phase and a number of parameters with correlations ranging from −0.423 to 0.421 rho. The highest positive correlation was the parameter Teta2, which demonstrated a rho=0.421, $p<0.001$. There were also several texture features derived from the arterial phase showing significant correlations with Ki67 LI (rho: from −0.258 to 0.292). For T2WI and PVP, the correlation coefficient ranged from −0.301 to 0.284 and 0.240 to 0.282, respectively.

Tissue classification results across the four phases are exhibited in Table 5. Only 82 samples were included in T2WI

Table 3
MRI features.

Variable	Low Ki67 group (n=25)	High Ki67 group (n=58)	p-Value
Tumor size (cm)[a]	4.38±2.76	6.39±3.97	0.026
Arterial phase hyperenhancement			0.991
Present	21 (25.3)	47 (56.6)	
Absent	4 (4.8)	11 (13.3)	
Washout			0.274
Present	20 (24.1)	53 (63.9)	
Absent	5 (6.0)	5 (6.0)	
Enhancing capsule			0.07
Present	14 (16.9)	44 (53.0)	
Absent	11 (13.2)	14 (16.9)	
Restricted diffusion			0.145
Present	18 (21.7)	51 (61.5)	
Absent	7 (8.4)	7 (8.4)	
Mild-moderate T2 hyperintensity			0.079
Present	22 (26.5)	57 (68.7)	
Absent	3 (3.6)	1 (1.2)	
Haemorrhage			0.003
Present	1 (1.2)	23 (27.7)	
Absent	24 (28.9)	35 (42.2)	
Intralesional fat			0.359
Present	3 (3.6)	3 (3.6)	
Absent	22 (26.5)	55 (66.3)	
Hepatobiliary phase hypointensity			0.301
Present	24 (28.9)	58 (69.9)	
Absent	1 (1.2)	0 (0)	

Unless otherwise indicated, data are numbers of patients, with percentage in parentheses.
[a] Data are means±standard deviation.

due to the detection of obvious artefacts in one sample. The NDA of texture features was excellent, with misclassification rates from 6.02% to 8.43% regardless of the phase analysed. For LDA, the misclassification rates of HBP, AP, and PVP (misclassification rates ranged between 9.64–15.66%) were superior to the result observed in T2WI (misclassification rate 25.61%). A plot of LDA and NDA based on HBP is shown in Fig 4, revealing good to excellent results. The fair-to-poor classification results were obtained from the RA and PCA across all scanning phases.

Discussion

HCCs with higher Ki67 LI indicate faster growth and poorer prognosis.[11,14] The nuclear Ki67 protein is associated with cell proliferative activity, which may be indicative of tumour aggressiveness. It is expressed in all phases of the cell cycle except G0, with particularly high expression observed in the G2/M phase.[28] In the present study, a significant correlation was demonstrated between tumour size and the Ki67 index, indicating that larger tumours had higher Ki67 LI.[29] Histological grades were also significantly different between the two groups (high versus low Ki67), suggesting that HCCs with higher Ki67 LI tend to display a lower differentiation pattern. These findings are agreeable with previous research.[11] In this study, haemorrhage was significantly different between groups, although this finding is not consistent with a recent study.[30] Possible reasoning for the incompatible results may lie in inherent and technical inconsistencies between the two groups of observers. Thus, further study is necessary to replicate this finding. Unexpectedly, no other morphological features examined demonstrated statistically significant differences between the low and high Ki67 groups, including the contrast enhancement imaging.

In this study, texture analysis (a quickly growing application in medical imaging) was used to demonstrate whether texture features can accurately differentiate between low and high Ki67 expressing groups using standard

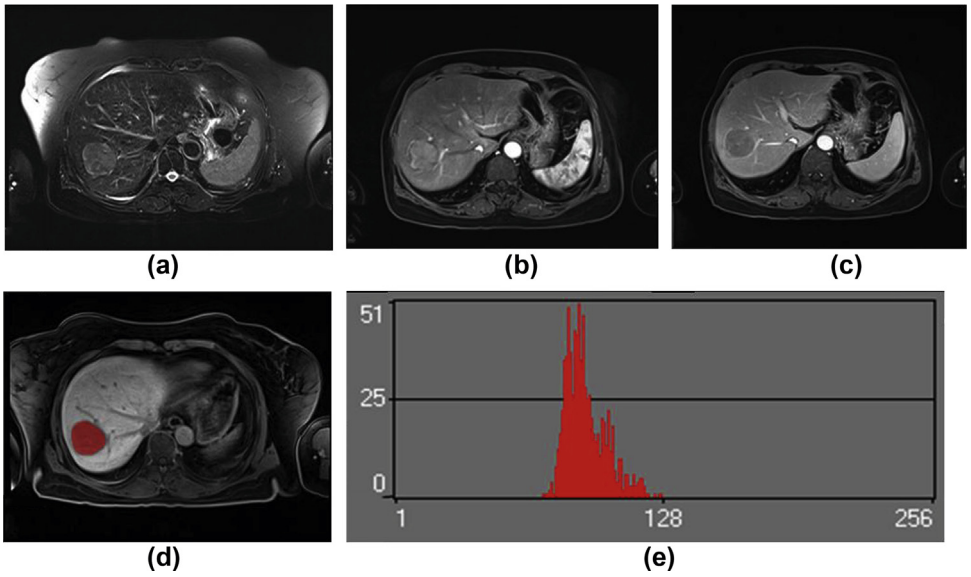

Figure 2 HCC with Ki67 LI of 8% in a 60-year-old female patient. The lesion shows slightly high signal intensity on T2WI (a), hyper-enhancement in the arterial phase (b), and wash-out in the portal venous phase (c). The ROI and the histogram map derived from the hepatobiliary phase is shown in (d) and (e).

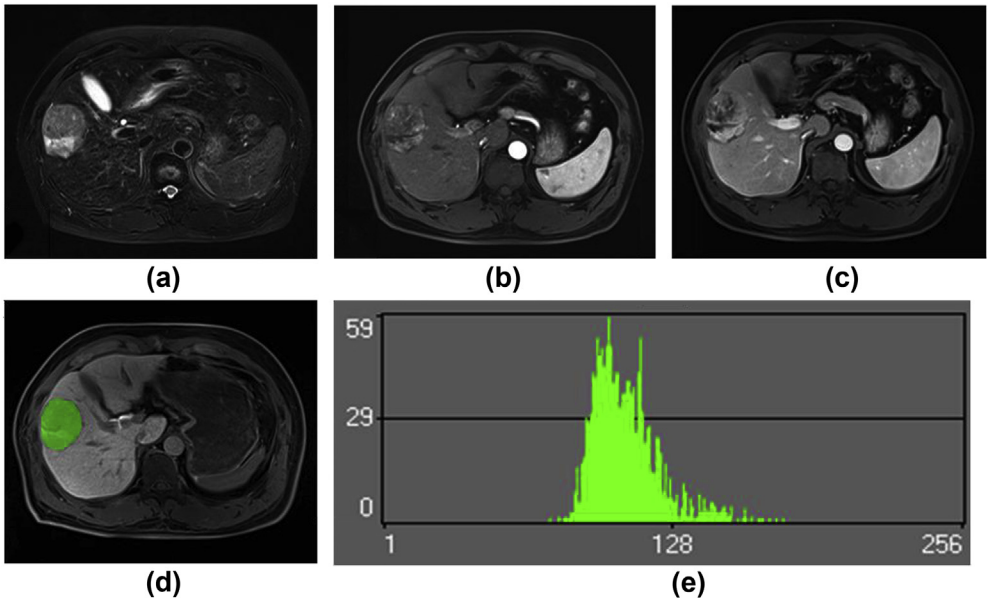

Figure 3 HCC with Ki67 LI of 40% in a 50-year-old male patient. The lesion also shows slightly high signal intensity in T2WI (a). From the arterial phase (b) and portal venous phase (c), the lesion shows the typical appearance of HCC. The region of interest put on the hepatobiliary phase (d) and the histogram map (e) indicate the parameter "Variance" "Perc.90%" and "Perc.99%" is statistical significantly between the two groups.

MRI. Texture analysis has demonstrated previous success in reflecting histological subtypes in breast cancer, thyroid cancer, and others.[29,31] To date, however, the potential of texture analyses derived from the HBP, T2WI, AP, and PVP (the most relevant sequences used in HCC diagnosis) to predict Ki67 LI, a biomarker reflecting the proliferation status of tumours,[10,11] has not been explored. From this research, it was found that histogram-derived parameters including variance, Perc.90% and Perc.99% of HBP were positively correlated with Ki67 LI (rho: 0.252–0.272). This suggested that the signal intensity in HBP imaging was detectably higher in the high Ki67 expressing group such that the grey-scale of the image changes greatly, which can facilitate visualisation of Ki67 (Figs 2 and 3). The five texture parameters derived from the GLRLM of HBP were noticeably different, where signal intensity was more heterogeneous in given directions such as horizontal, vertical, in the high Ki67 group. HCCs with high Ki67 LI may appear more heterogeneous due to the internal structure of neoplasm,

Table 4
Correlation between 30 texture features and Ki67, which were statistical significantly.

Parameter	HBP-rho	*p*-Value	Parameter	T2WI-rho	*p*-Value	Parameter	AP-rho	*p*-Value	Parameter	PVP-rho	P Value
Variance	0.272	0.0125	Skewness	−0.261	0.0177	Skewness	0.409	<0.001	S(0,5)SumVarnc	0.24	0.0288
Perc.90%	0.252	0.0214	S(0,1)SumAverg	0.247	0.0254	S(3,−3)Contrast	−0.285	0.009	Horzl_RLNonUni	0.282	0.0099
Perc.99%	0.271	0.0133	S(1,1)SumAverg	0.2199	0.0471	S(3,−3)Correlat	0.299	0.0059	135dr_RLNonUni	0.272	0.0129
S(5,-5)SumAverg	−0.258	0.0187	S(0,2)SumAverg	0.281	0.0104	S(3,−3)SumVarnc	0.275	0.0118			
Horzl_RLNonUni	0.292	0.0075	S(0,3)SumAverg	0.284	0.0098	S(3,−3)DifVarnc	−0.269	0.0141			
Horzl_GLevNonU	0.277	0.0111	S(0,4)SumAverg	0.219	0.0482	S(0,4)Contrast	−0.259	0.0182			
Vertl_RLNonUni	0.282	0.0099	S(4,4)Contrast	−0.219	0.0483	S(0,4)Correlat	0.262	0.0167			
45dgr_RLNonUni	0.275	0.0118	S(4,4)InvDfMom	0.245	0.0268	S(0,4)DifVarnc	−0.261	0.0172			
135dr_RLNonUni	0.272	0.0129	S(4,4)SumAverg	0.218	0.0495	S(0,4)DifEntrp	−0.249	0.0233			
			S(5,5)SumAverg	0.275	0.0125	S(5,0)Contrast	−0.225	0.0411			
			WavEnHH_s-2	−0.245	0.0268	S(5,0)Correlat	0.238	0.0304			
			WavEnHH_s-3	-0.301	0.0064	S(5,0)SumAverg	−0.233	0.0336			
						S(5,0)DifEntrp	-0.219	0.0465			
						S(0,5)Contrast	-0.254	0.0203			
						S(0,5)Correlat	0.272	0.0129			
						S(0,5)DifVarnc	-0.249	0.0233			
						S(5,-5)Correlat	0.258	0.0187			
						Teta1	-0.423	<0.001			
						Teta2	0.421	<0.001			
						WavEnLH_s-1	-0.323	0.0028			
						WavEnLH_s-2	-0.337	0.0019			

HBP, hepatobiliary phase; T2WI, T2-weighted imaging; AP, arterial phase; PVP, portal venous phase.

Table 5
Misclassification results in groups of the four phase images.

Phase	HBP (n=83)	T2WI (n=82)	AP (n=83)	PVP (n=83)
RDA	36.14% (25.9%,47.4%)	45.12% (33.7%,55.9%)	51.81% (40.6%,62.9%)	49.40% (38.2%,60.6%)
PCA	43.37% (32.5%,54.7%)	42.68% (31.4%,53.5%)	48.19% (37.1%,59.4%)	40.96% (30.3%,52.3%)
LDA	15.66% (8.6%,25.3%)	25.61% (16.4%,36%)	10.84% (5.1%,19.6%)	9.64% (4.3%,18.1%)
NDA	8.43% (3.5%,16.6%)	7.32% (2.7%,15.1%)	6.02% (2%,13.5%)	8.43% (3.5%,17%)

Data are misclassification rates, with 95% confidence interval in parentheses.
HBP, hepatobiliary phase; T2WI, T2-weighted imaging; AP, arterial phase; PVP, portal venous phase.
RDA, raw data analysis; PCA, principal component analysis; LDA, linear discriminant analysis; NDA, nonlinear discriminant analysis.

which may be associated with faster growth in high Ki67 expressing groups.

For T2WI, the histogram-derived parameter "skewness" showed a significant negative correlation. Skewness is a digital feature that represents the asymmetric degree of statistical data distribution. The present findings revealed that the signal intensity was more asymmetrically distributed in the low Ki67 expressing group based on T2WI. On the other hand, this parameter demonstrated a significant positive correlation in AP (rho=0.409, $p<0.001$), meaning signal intensity is more asymmetrically distributed (right skewed) in the high Ki67 expressing group after contrast medium administration. This showed that the grey value of AP images was relatively low in the high Ki67 expressing group compared with the low Ki67 expressing group; however, this finding is inconsistent with a previous study by Hu *et al.*,[30] which showed that skewness was not significantly correlated with Ki67 expression in AP. Other histogram-derived parameters, including mean, median, etc., were also different from the study of Hu *et al.*; incongruent use of software and/or methodology could be the reasoning for this observation. As such, further study is needed to replicate the present findings. The most frequently significant texture parameter in this study was the SumAverg derived from GLCOM in T2WI.

The SumAverg is a measurement of average grey value of image pixels, indicating degree of brightness. The findings of the present suggested that the signal intensity is slightly brighter in high Ki67 group compared to the low Ki67 group. This may be indicative of cystic degeneration or necrosis caused by relative insufficient blood supply in the procedure of faster growth. Contrast and Correlat were also frequently significant parameters derived from GLCOM in AP images, where the Contrast displayed a negative correlation and the other one positive. Contrast reflects the clarity of the image and the depth of texture grooves. The greater the Contrast, the deeper the texture groove, and the clearer the visual effect. In this study, the AP images were clearer in the low Ki67 expressing group. Correlat, on the other hand, reflects the correlation of the local grey-scale between image pixels. When the local grey-scale of image pixels is uniformly equal, the correlation is greater.

In sum, texture analysis using MaZda software provides a quantitative method for image analysis.[24,25] Humans are conditioned to assess texture only qualitatively, while often significant quantitative analysis is weighted to obtain objective and reliable diagnostic information[24]; however, a textural quantitative analysis may carry substantial information about the structure of images, such as brightness, roughness, directivity, randomness, smoothness, granulation, etc. In total, there are almost 300 textural features evaluated based on image histogram, gradient, co-occurrence matrix, run-length matrix, autoregressive model, and Haar wavelet.[24] Clinicians may obtain different and valuable information from diagnostic images, which potentially reflects histopathological parameters of a tumour.[29,31] Several studies have applied textural analysis for the identification of evolving pathologies including liver fibrosis[20] and advanced HCC.[32] The present study attempted to use texture analysis to identify the proliferation status of HCCs. The misclassification results generated from HBP, T2WI, AP, and PVP were rated excellent to good (by

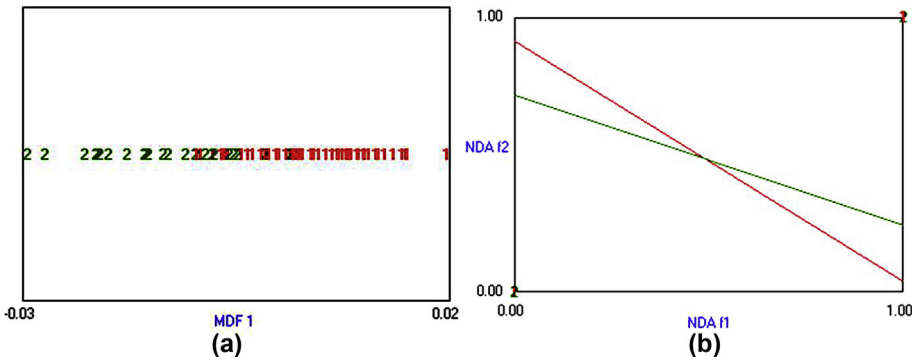

Figure 4 (a) LDA of the low and high Ki67 group on hepatobiliary phase images. (b) NDA of the two groups on hepatobiliary phase images: 1, the low Ki67 group; 2, the high Ki67 group.

LDA and NDA) except for a moderate rating from T2WI (by LDA). Procedures were implemented in the B11 module to include PCA, LDA, and NDA based on the selected 30 texture features.[25] The classification method used here is worth noting. Although LDA is a conventional approach and a more straightforward method, it is important to integrate and test more advanced methods like the 1-NN classifier, which may substantially improve classification (as in this study). The artificial neural network classifier was also used herein for features resulting from NDA.[33] It is a data-driven, self-adaptive method, which can adjust to the data and generate more flexible nonlinear models denoting complex relationships. When datasets are linearly separable, LDA has performed well; however, when non-linearity is present, the classification accuracy decreases. Within real datasets, the degree of non-linearity is often unknown. Thus the utilisation of both LDA and NDA to compare performance is useful.[34]

Some limitations to address include the retrospective nature of the present study. Despite having selected samples according to strict inclusion and exclusion criteria, selection bias may not be avoided. Second, texture analysis was not performed in advanced imaging with ADC, which is widely used in clinical practice.[35] In this study, multiple phase images were evaluated, particularly HBP. Third, the ROI was manually selected from the section with the largest proportion of lesion, which may have caused loss of volumetric information. On the other hand, a 3D method is probably not suitable for clinical use due to the cumbersome nature of the accompanying procedures. Overall, enough texture features could be obtained from the largest section. Although in this study cases were stratified according to the expression of Ki67 $>10\%$ and Ki67 $\leq 10\%$, other studies have chosen different cut-off values.[14] Finally, due to the relatively small samples, a k-fold cross-validation was not undertaken. In future, a larger data set will be needed to evaluate the model more robustly. At that point, morphological features can also be included in the analysis to improve the accuracy of identification.

In conclusion, the present results suggest that texture analysis of HBP, T2WI, AP, and PVP may be used for discriminating Ki67 proliferation status in HCCs. These MRI texture features may directly or indirectly reveal underlying structures similar to traditional histopathology. Therefore, this strategy may provide useful preoperative information beneficial to establishing a treatment plan. Moreover, during the monitoring and follow-up of HCC during and after treatment, this novel application may also offer a non-invasive alternative.

Conflicts of interest

The authors declare no conflict of interest.

Acknowledgements

This study has received funding from the Fujian Provincial Health and Family Planning Commission (CN; award number: 2017-CX-27), Fujian Provincial Department of Science and Technology (CN; award number: 2015J0105), and Fujian Medical Elite Cultivation Program (CN; award number: 2015-ZQN-ZD-19).

References

1. Forner A, Reig M, Bruix J. Hepatocellular carcinoma. *Lancet* 2018;**391**(10127):1301–14.
2. Zimmerman MA, Ghobrial RM, Tong MJ, *et al*. Recurrence of hepatocellular carcinoma following liver transplantation: a review of preoperative and postoperative prognostic indicators. *Arch Surg* 2008;**143**(2):182–8. discussion 8.
3. Imamura H, Matsuyama Y, Tanaka E, *et al*. Risk factors contributing to early and late phase intrahepatic recurrence of hepatocellular carcinoma after hepatectomy. *J Hepatol* 2003;**38**(2):200–7.
4. Llovet JM, Schwartz M, Mazzaferro V. Resection and liver transplantation for hepatocellular carcinoma. *Semin Liver Dis* 2005;**25**(2):181–200.
5. Portolani N, Coniglio A, Ghidoni S, *et al*. Early and late recurrence after liver resection for hepatocellular carcinoma: prognostic and therapeutic implications. *Ann Surg* 2006;**243**(2):229–35.
6. Wakayama K, Kamiyama T, Yokoo H, *et al*. Huge hepatocellular carcinoma greater than 10 cm in diameter worsens prognosis by causing distant recurrence after curative resection. *J Surg Oncol* 2017;**115**(3):324–9.
7. An C, Kim DW, Park YN, *et al*. Single hepatocellular carcinoma: preoperative MR imaging to predict early recurrence after curative resection. *Radiology* 2015;**276**(2):433–43.
8. Lee JM, Jang BK, Lee YJ, *et al*. Survival outcomes of hepatic resection compared with transarterial chemoembolization or sorafenib for hepatocellular carcinoma with portal vein tumour thrombosis. *Clin Mol Hepatol* 2016;**22**(1):160–7.
9. Xu XL, Liu XD, Liang M, *et al*. Radiofrequency ablation versus hepatic resection for small hepatocellular carcinoma: systematic review of randomized controlled trials with meta-analysis and trial sequential analysis. *Radiology* 2018;**287**(2):461–72.
10. Sherr CJ. Cancer cell cycles. *Science* 1996;**274**(5293):1672–7.
11. Shi W, Hu J, Zhu S, *et al*. Expression of MTA2 and Ki-67 in hepatocellular carcinoma and their correlation with prognosis. *Int J Clin Exper Pathol* 2015;**8**(10):13083–9.
12. Nakanishi K, Sakamoto M, Yamasaki S, *et al*. Akt phosphorylation is a risk factor for early disease recurrence and poor prognosis in hepatocellular carcinoma. *Cancer* 2005;**103**(2):307–12.
13. Luo Y, Ren F, Liu Y, *et al*. Clinicopathological and prognostic significance of high Ki-67 labeling index in hepatocellular carcinoma patients: a meta-analysis. *Int J Clin Exper Med* 2015;**8**(7):10235–47.
14. Li HH, Qi LN, Ma L, *et al*. Effect of KI-67 positive cellular index on prognosis after hepatectomy in Barcelona Clinic Liver Cancer stage A and B hepatocellular carcinoma with microvascular invasion. *OncoTargets Ther* 2018;**11**:4747–54.
15. El-Serag HB, Marrero JA, Rudolph L, *et al*. Diagnosis and treatment of hepatocellular carcinoma. *Gastroenterology* 2008;**134**(6):1752–63.
16. European Association for the Study of the Liver. EASL clinical practice guidelines: management of hepatocellular carcinoma. *J Hepatol* 2018;**69**(1):182–236.
17. Incoronato M, Aiello M, Infante T, *et al*. Radiogenomic analysis of oncological data: a technical survey. *Int J Mol Sci* 2017;**18**(4).
18. Hossain S, Serikawa S. Texture databases — a comprehensive survey. *Pattern Recog Lett* 2013;**34**(15):2007–22.
19. Castellano G, Bonilha L, Li LM, *et al*. Texture analysis of medical images. *Clin Radiol* 2004;**59**(12):1061–9.
20. Bahl G, Cruite I, Wolfson T, *et al*. Noninvasive classification of hepatic fibrosis based on texture parameters from double contrast-enhanced magnetic resonance images. *J Magn Reson Imaging* 2012;**36**(5):1154–61.
21. Chamming's F, Ueno Y, Ferre R, *et al*. Features from computerized texture analysis of breast cancers at pretreatment MR imaging are associated with response to neoadjuvant chemotherapy. *Radiology* 2018;**286**(2):412–20.

22. Yan L, Liu Z, Wang G, *et al*. Angiomyolipoma with minimal fat: differentiation from clear cell renal cell carcinoma and papillary renal cell carcinoma by texture analysis on CT images. *Acad Radiol* 2015;**22**(9):1115–21.
23. Kielar AZ, Chernyak V, Bashir MR, *et al*. LI-RADS 2017: an update. *J Magn Reson Imaging* 2018;**47**(6):1459–74.
24. Sheftel M. A software tool for automatic classification and segmentation of 2D/3D medical images. *Nucl Inst Meth Phys Res A* 2013;**702**(2):137–40.
25. Szczypinski PM, Strzelecki M, Materka A, *et al*. MaZda—a software package for image texture analysis. *Comput Methods Prog Biomed* 2009;**94**(1):66–76.
26. Szczypinski PM, Strzelecki M, Materka A. MaZda—a software for texture analysis. In: *International symposium on information Technology convergence*; 2007. p. 245–9.
27. Huang Z, Xu X, Meng X, *et al*. Correlations between ADC values and molecular markers of Ki-67 and HIF-1alpha in hepatocellular carcinoma. *Eur J Radiol* 2015;**84**(12):2464–9.
28. Gerdes J, Lemke H, Baisch H, *et al*. Cell cycle analysis of a cell proliferation-associated human nuclear antigen defined by the monoclonal antibody Ki-67. *J Immunol* 1984;**133**(4):1710–5.
29. Holli-Helenius K, Salminen A, Rinta-Kiikka I, *et al*. MRI texture analysis in differentiating luminal A and luminal B breast cancer molecular subtypes — a feasibility study. *BMC Med Imag* 2017;**17**(1):69.
30. Hu XX, Yang ZX, Liang HY, *et al*. Whole-tumour MRI histogram analyses of hepatocellular carcinoma: correlations with Ki-67 labeling index. *J Magn Reson Imag* 2017;**46**(2):383–92.
31. Meyer HJ, Schob S, Hohn AK, *et al*. MRI texture analysis reflects histopathology parameters in thyroid cancer — a first preliminary study. *Translat Oncol* 2017;**10**(6):911–6.
32. Mule S, Thiefin G, Costentin C, *et al*. Advanced hepatocellular carcinoma: pretreatment contrast-enhanced CT texture parameters as predictive biomarkers of survival in patients treated with sorafenib. *Radiology* 2018;**288**(2):445–55.
33. Holli K, Laaperi AL, Harrison L, *et al*. Characterization of breast cancer types by texture analysis of magnetic resonance images. *Acad Radiol* 2010;**17**(2):135–41.
34. Orphanidou-Vlachou E, Vlachos N, Davies NP, *et al*. Texture analysis of T1- and T2-weighted MR images and use of probabilistic neural network to discriminate posterior fossa tumours in children. *NMR Biomed* 2014;**27**(6):632–9.
35. Razek AA, Massoud SM, Azziz MR, *et al*. Prediction of esophageal varices in cirrhotic patients with apparent diffusion coefficient of the spleen. *Abdom Imag* 2015;**40**:1465–9.